1. Experimental section

Chemicals and Materials

All the chemicals were used as received. $Ni(NO_3)_2·6H_2O$ (analytical reagent, AR), $Co(NO_3)_2·6H_2O$ (AR), $FeSO_4·7H_2O$ (AR), $Cr(NO_3)_3·9H_2O$ (AR), $Zr(NO_3)_4·5H_2O$ (AR), HNO (AR), and L-Thioproline (AR), all purchased from Shanghai Aladdin Biochemical Technology Co., Ltd. Ketjen Black (EC-300J) was obtained from Suzhou Sinero Technology Co., Ltd. Nickel foam (thickness: 1.5 mm, areal density: 320 $g·m^{-2}$,purity:99.8%) was supplied by Kunshan Guangjiaoyuan New Materials Co., Ltd. 24K heat-resistant carbon fiber was procured from Yuannuo Antistatic & Cleanroom Products Co., Ltd. Silver conductive paste was acquired from Guangzhou Kaixiang Electronics Co., Ltd., and copper foil tape was sourced from Xinhongsen Office Supplies Co., Ltd.

Pretreatment of Ketjen Black

1 g of Ketjen Black was placed in a 250 mL round-bottom flask. Then, 100 mL of concentrated nitric acid was added. The flask was subjected to ultrasonic treatment for 30 min. Subsequently, the flask was heated to 85 °C and maintained at this temperature for 1 h. The product was washed four times with water and collected by vacuum filtration. Finally, the resulting solid was lyophilized for 12 h to obtain the treated Ketjen black.

Preparation of the HES catalysts

0.75 mmol of $Ni(NO_3)_2·6H_2O$, 0.25 mmol of $Co(NO_3)_2·6H_2O$, 0.25 mmol of $FeSO_4·7H_2O$, 0.25 mmol of $Cr(NO_3)_3·9H_2O$, 0.25 mmol of $Zr(NO_3)_4·5H_2O$ 182 mg of treated Ketjen Black, and 3 mmol of L-thioproline was placed into a 50 mL beaker. 20 mL of deionized water, as well as 0.4 mL of 0.5 M sulfuric acid were added with stirring. The beaker was sonicated for 30 min, and then heated in an oil bath at 85 °C with stirring until a slurry was obtained.

Approximately 20 mg of the slurry was uniformly coated onto the carbon thermal shock substrate. The substrate was a 7.5 cm-long heat-resistant carbon fiber, which was bonded with copper foil tape (7 cm × 2 cm) on each side using silver conductive paste as binder. The slurry coated substrate was then transferred into a custom cylindrical chamber, which was purged with N_2 for 10 min to establish an inert atmosphere. A DC power supply was connected with the substrate through the copper foil tape, and activated at 22 A for 3 s to perform the carbothermal shock process. After the reaction, the resulting (NiFeCoCrZr)S/C powder was scraped off and collected.

The mono-, bi-, tri-, and tetra-metallic sulfide catalysts were prepared using similar process with the metal source for all the catalysts are kept as each added amount the same. The amount of Ni source is kept as 0.75 mmol and the other metal are kept as 0.25 mmol each. L-thioproline was added at a molar ratio of M:T = 1:1.71, and carbon was incorporated at a mass ratio of M:C = 3:5. The detailed amounts used in the synthesis are summarized in Table S1.

Electrochemical Measurements

Electrochemical tests were conducted using a CHI-760 electrochemical workstation in a standard three-electrode system. The working electrode was prepared by casting the catalyst onto a glassy carbon electrode or nickel foam. 3 mg of the catalyst was dispersed in a mixture of 0.9 mL of isopropanol, 0.085 mL of deionized water, and 0.015 mL of 5 wt% Nafion solution to form a catalyst ink. Then, 32.7 μL of the ink was drop-cast onto a glassy carbon electrode with a diameter of 0.5 cm. For stability test, the ink was prepared by mixing 3 mg of the catalyst with 0.9 mL of isopropanol, 0.076 mL of deionized water, and 0.024

mL of 5 wt% Nafion solution, and 333 μL of the ink was deposited onto a nickel foam substrate (1 cm × 1 cm). A Hg/HgO electrode is used as the reference electrode and a carbon rod was served as counter electrode. The electrochemical measurements were carried out in O_2-saturated 1 M KOH electrolyte at 30 °C. All potentials were referenced to the reversible hydrogen electrode (RHE).

Polarization curves were obtained via linear sweep voltammetry (LSV) at a scan rate of 5 $mV \cdot s^{-1}$ with 100% iR compensation. Electrochemical impedance spectroscopy (EIS) was performed in the frequency range from 100 kHz to 0.1 Hz. The OER stability was evaluated through chronopotentiometry at a current density of 100 $mA \cdot cm^{-2}$.

AEMWE Performance

Membrane electrode assemblies (MEAs) were fabricated using the catalyst-coated substrate (CCS) technique. The cathode was prepared by spraying PtRu/C (40%Pt and 20%Ru) catalyst ink (3 $mg \cdot mL^{-1}$) onto carbon paper (HCP030N). The anode was fabricated by depositing the synthesized (NiFeCoCrZr)S/C ink (4 $mg \cdot mL^{-1}$) onto nickel felt. Both electrodes had a geometric area of 4 cm^2. The catalyst loading was 1 $mg \cdot cm^{-2}$ for the anode, and 0.3 $mg_{Pt} \cdot cm^{-2}$ plus 0.15 $mg_{Ru} \cdot cm^{-2}$ for the cathode. PiperION™ membranes with thicknesses of 20 μm (for OER activity tests) and 40 μm (for stability tests) were used as the anion exchange membranes, which was rinsed in 1 M KOH for 2 h before use. The AEMWE cell was assembled using the membrane, catalyst layer, gas diffusion layers, stainless-steel flow field plates with a 4 cm^2 active area, and metallic bipolar plates. The cell performance was evaluated at 60 °C with 1 M KOH electrolyte circulating under ambient pressure. A loading of 1 $mg \cdot cm^{-2}$ was also applied for both IrO_2 and the (NiFeCoCrZr)S/C catalyst synthesized using untreated KB.

Characterization Techniques

Transmission electron microscopy (TEM, FEI Talos F200x) and scanning electron microscopy (SEM, Thermo scientific Apreo 2S) were used to examine the morphology and microstructure. X-ray diffraction (XRD, Rigaku D/Max 2500 VB2+/PC) was performed to identify the crystalline phases at a scan rate of $5° \cdot min^{-1}$ over a 2θ range of 10°–80°. X-ray photoelectron spectroscopy (XPS, Thermo Scientific K-Alpha) with an Al Kα excitation source was used to analyze the chemical states of elements. Inductively coupled plasma mass spectrometry (ICP-MS, Agilent 7800) was employed to determine the metal composition of the catalyst and the concentration of dissolved metal ions in solution. Differential electrochemical mass spectrometry (DEMS, QAS 100 Li) was utilized for in situ detection of isotopically labeled volatile products during electrocatalysis. For high-resolution morphological characterization of localized areas. Brunauer-Emmett-Teller Analyzer (BET, Micromeritics, ASAP 2460) was tested for Specific surface area and pore volume of the particles. Conductivity meter(CTA-3) was used to test the conductivity of the catalysts.

2. Figures

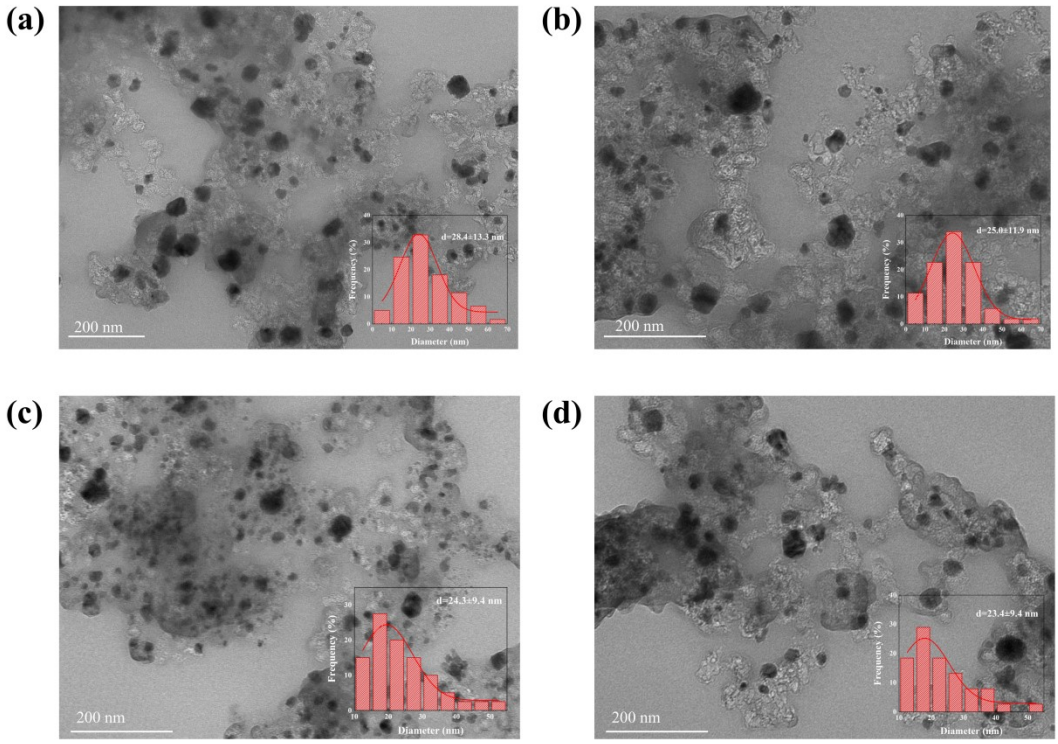

Figure S1 TEM images of (a) (NiFeCoCr)S/C, (b) (NiFeCo)S/C, (c) (NiFe)S/C, and (d) (Ni)S/C. Insets are the corresponding particle size distribution histograms.

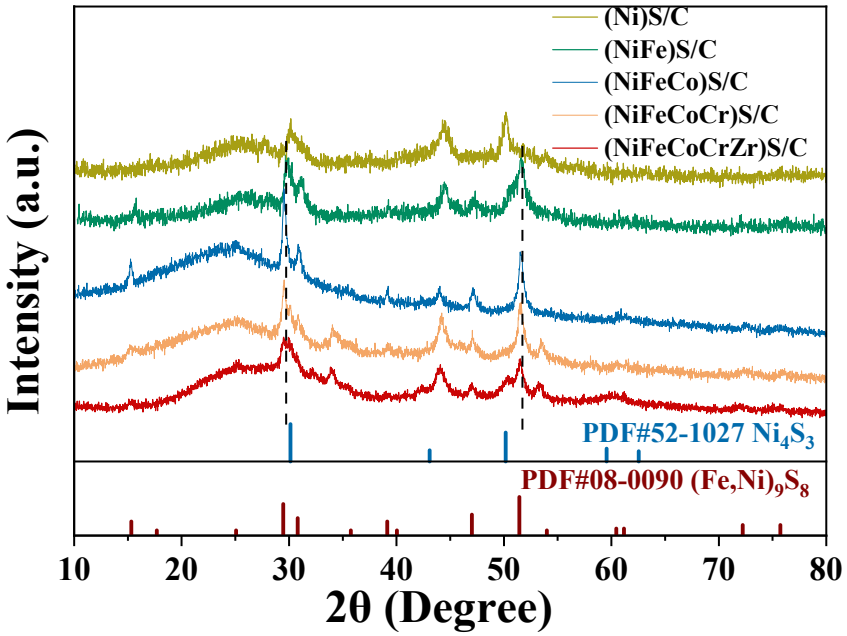

Figure S2 XRD patterns of (NiFeCoCrZr)S/C, (NiFeCoCr)S/C, (NiFeCo)S/C, (NiFe)S/C and (Ni)S/C.

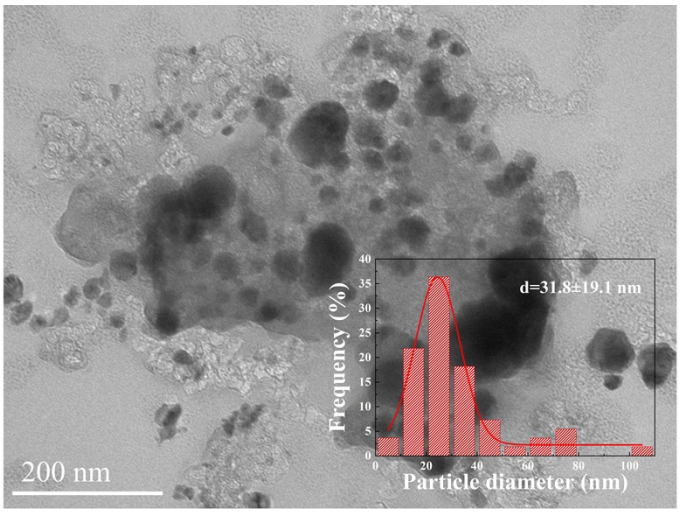

Figure S3 TEM image of the (NiFeCoCrZr)S/C catalyst synthesized using untreated Ketjen black. Inset is the corresponding particle size distribution histogram.

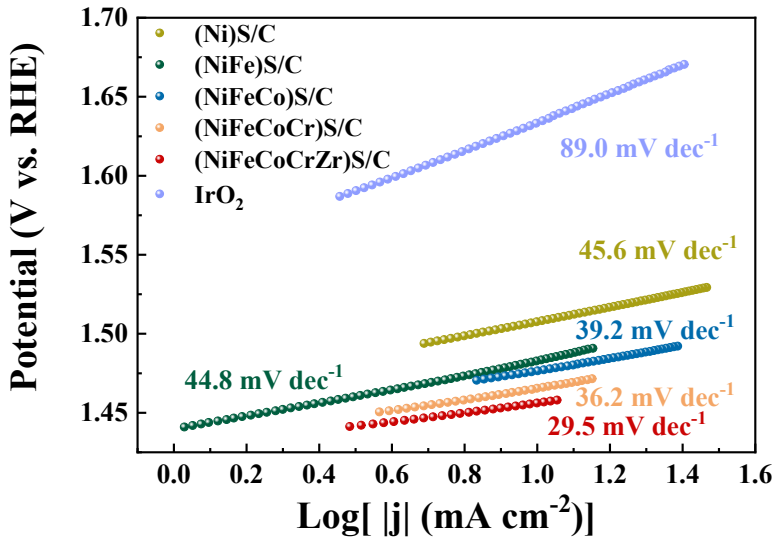

Figure S4 Tafel plots of the catalysts.

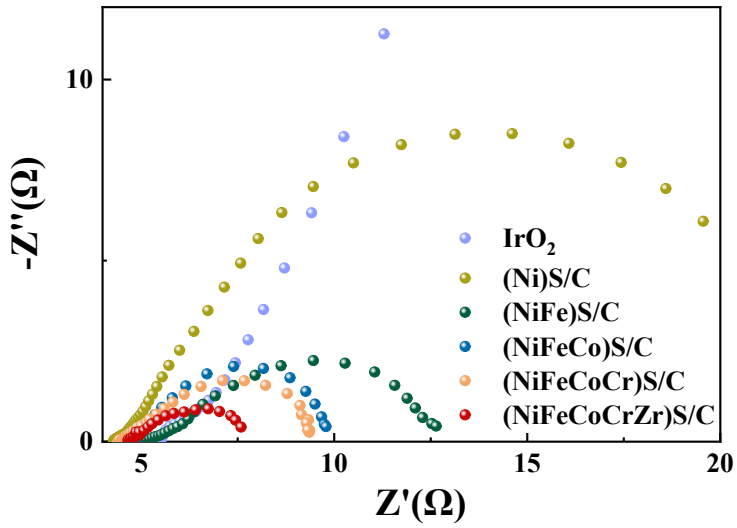

Figure S5 Nyquist plots of the catalysts.

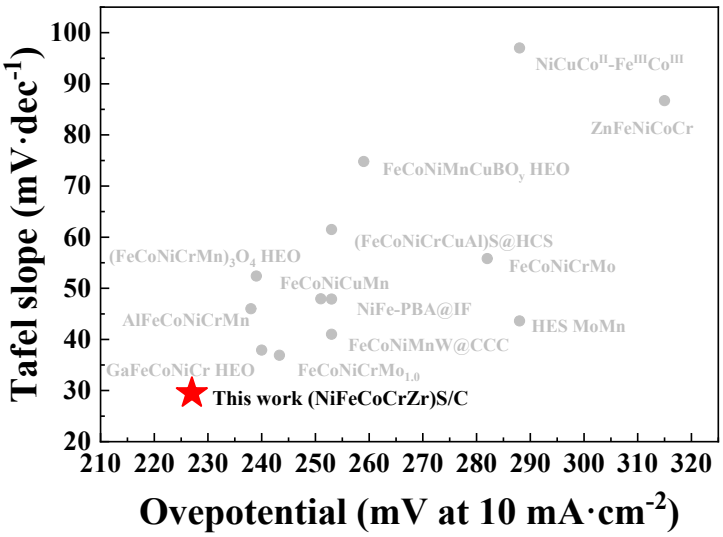

Figure S6 Summary of the overpotential at 10 mA·cm^{-2} and Tafel slope for (NiFeCoCrZr)S/C and recently reported high-entropy OER catalysts.

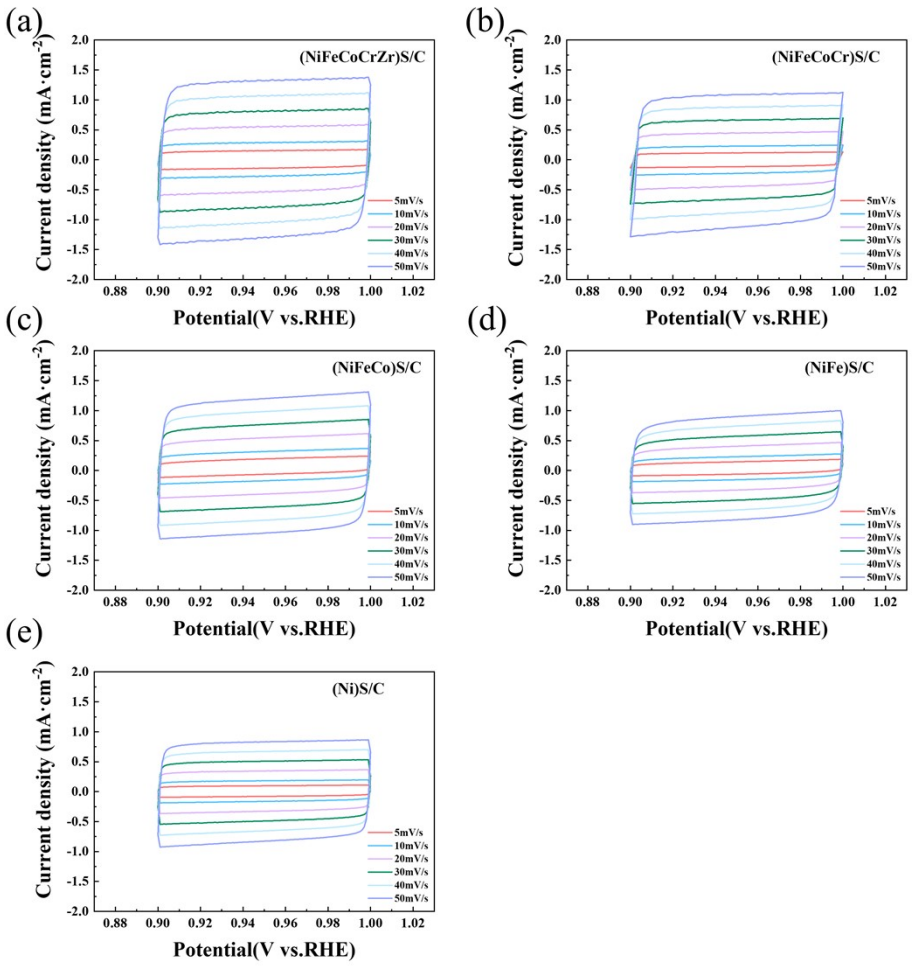

Figure S7 CV curves of the catalysts measured at different scan rates. (a) (NiFeCoCrZr)S/C. (b) (NiFeCoCr)S/C. (c) (NiFeCo)S/C. (d) (NiFe)S/C. (e) (Ni)S/C.

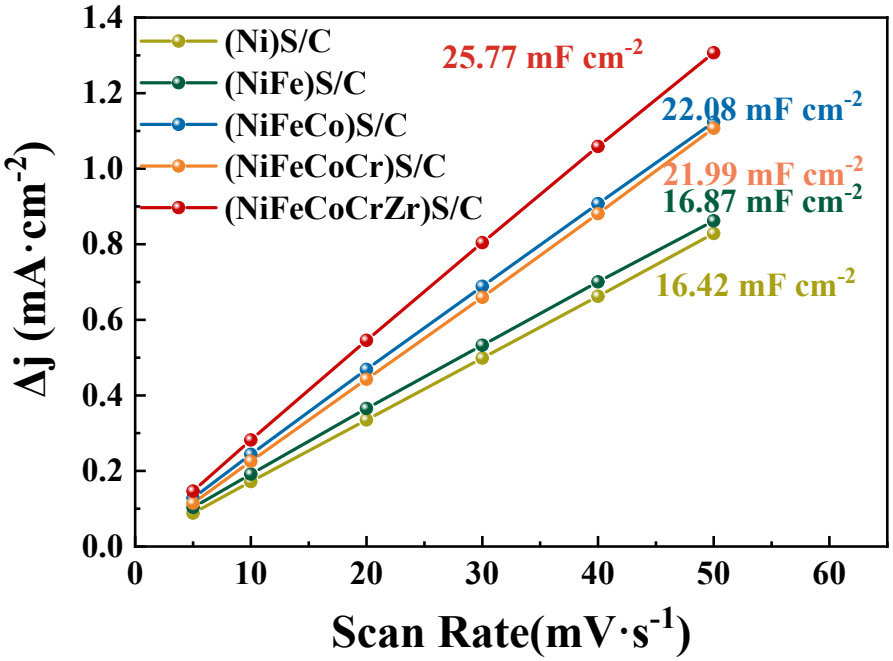

Figure S8 Double-layer capacitance (C_{dl}) of the catalysts.

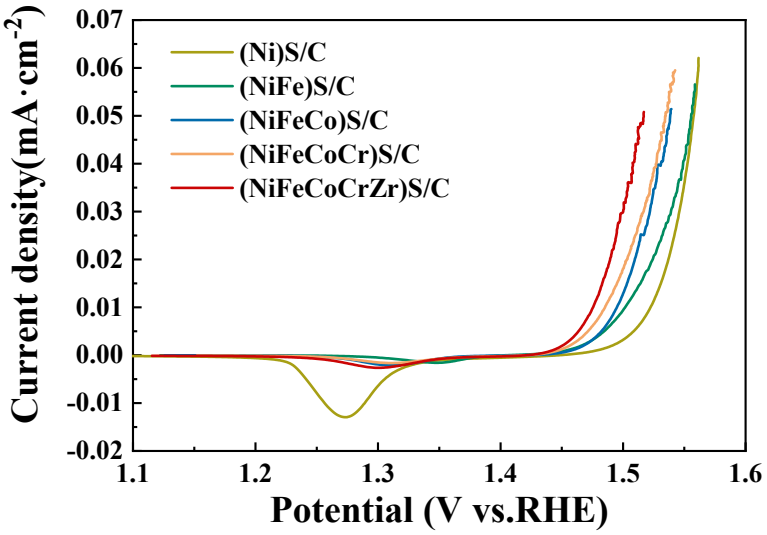

Figure S9 LSV curves of the catalyst normalized by the electrochemical active surface area (ECSA). A specific capacitance of 0.04 mF cm^{-2} was used for calculating the ECSA from the C_{dl}.

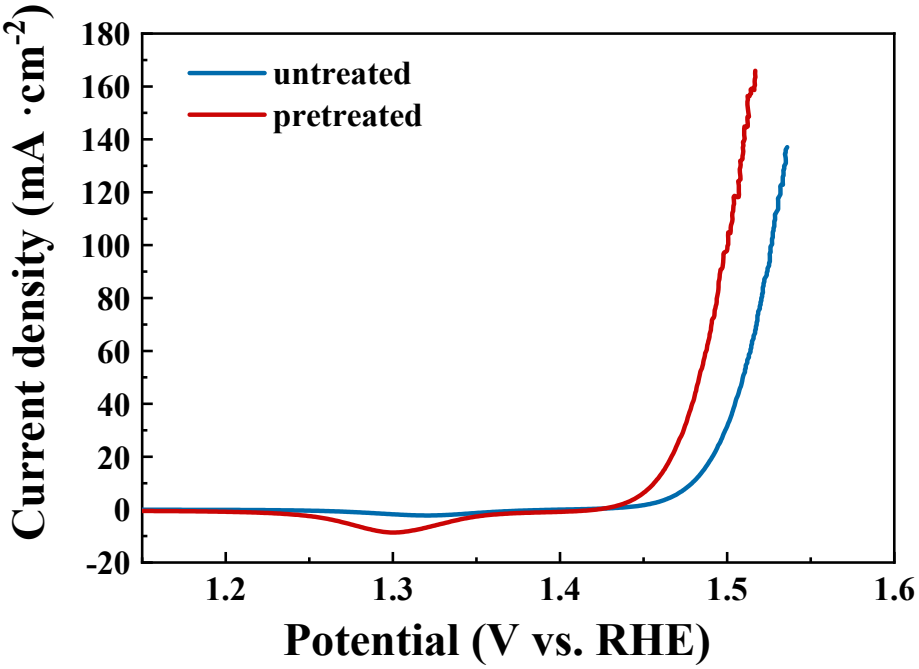

Figure S10 LSV curves of catalysts synthesized using pretreated and untreated Ketjen black at a scan rate of 5 $mV \cdot s^{-1}$ in 1 M KOH electrolyte (with iR compensation).

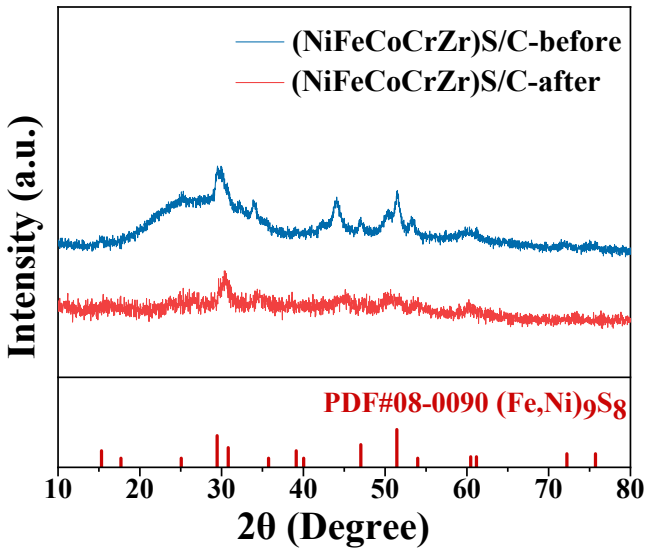

Figure S11 The XRD pattern of (NiFeCoCrZr)S/C before and after OER testing.

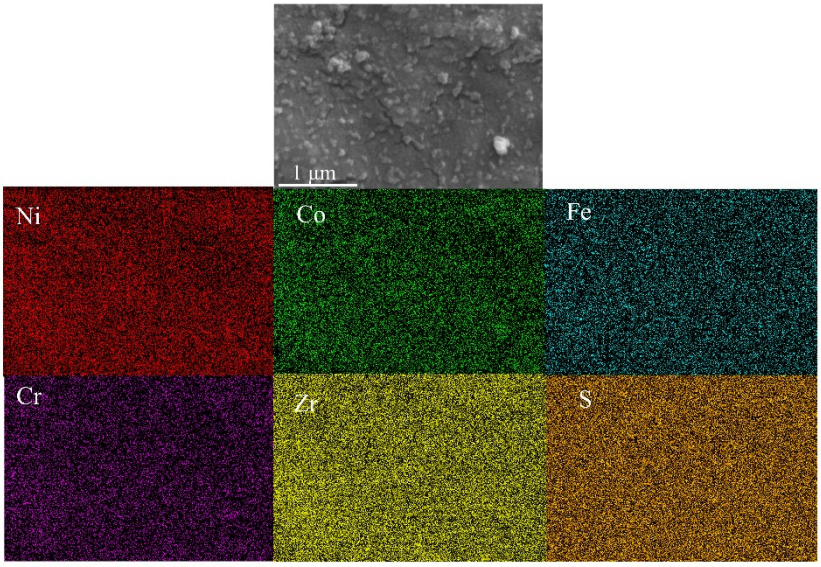

Figure S12 SEM image and EDS elemental mappings of (NiFeCoCrZr)S/C after OER testing.

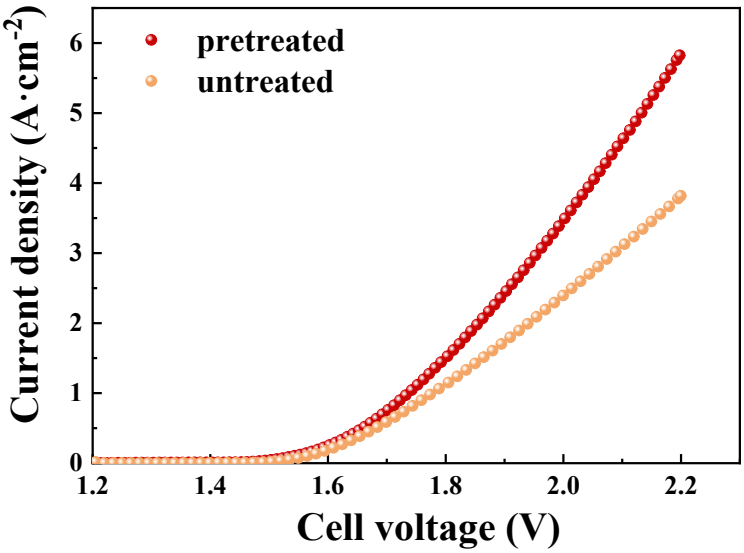

Figure S13 LSV curves of the AEMWE using (NiFeCoCrZr)S/C synthesized with pretreated and untreated carbon as anode. They were measured at the scan rate of 5 mV s^{-1} at 60°C with 1 M KOH feeding. The anode loading was 1 $mg_{Catalyst}$ cm^{-2} and the cathode was Pt-Ru/C with a loading of 0.45 mg_{PtRu} cm^{-2}. A 20 μm thick AEM was employed.

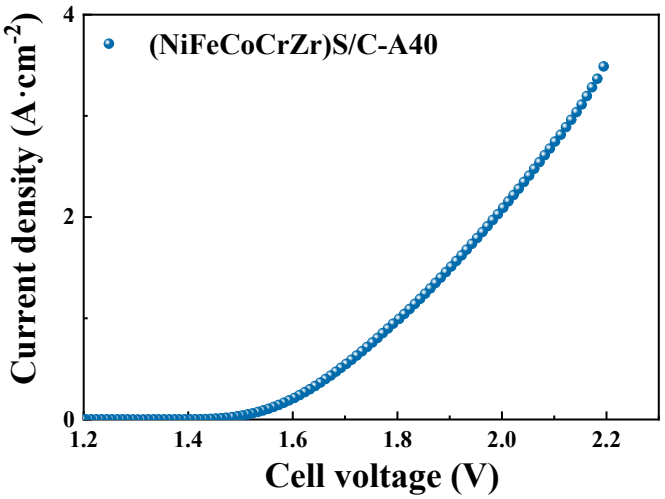

Figure S14 LSV curve the AEMWE measured at the scan rate of 5 $mV \cdot s^{-1}$ at 60°C with 1 M KOH feeding. The AEMWE was fabricated using (NiFeCoCrZr)S/C as anode with a loading of 1 $mg_{Catalyst} \cdot cm^{-2}$ and Pt-Ru/C as cathode with a loading of 0.45 $mg_{PtRu} \cdot cm^{-2}$. A 40 μm thick AEM was employed.

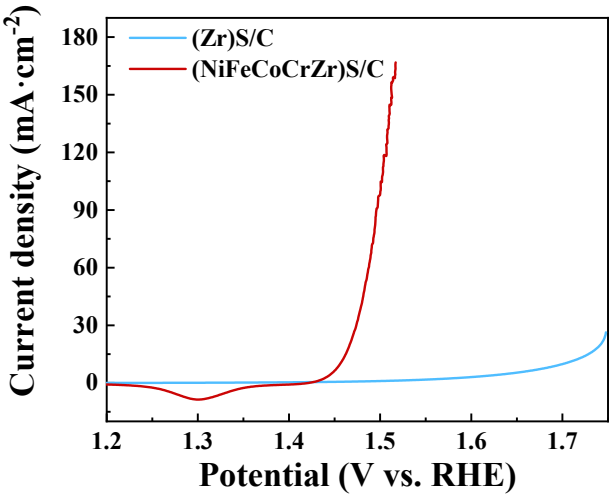

Figure S15 LSV curves of (Zr)S/C and (NiFeCoCrZr)S/C at a scan rate of 5 $mV \cdot s^{-1}$ in 1 M KOH electrolyte (with iR compensation).

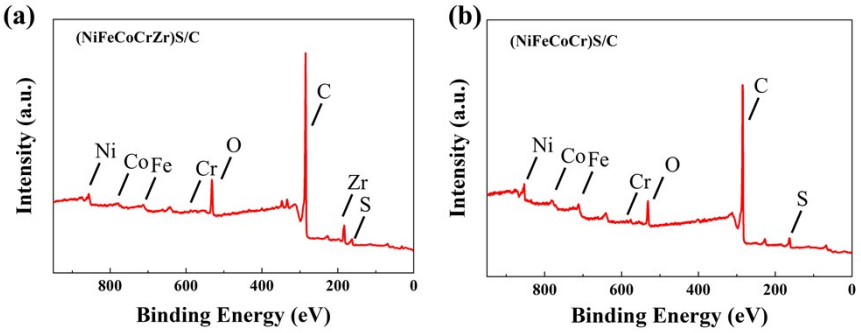

Figure S16 XPS survey spectra. (a) (NiFeCoCrZr)S/C. (b) (NiFeCoCr)S/C.

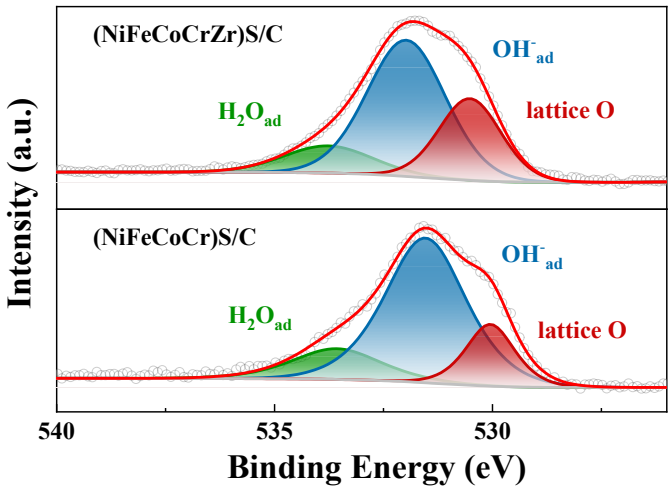

Figure S17 High-resolution O 1s core level XPS spectra of (NiFeCoCrZr)S/C and (NiFeCoCr)S/C.

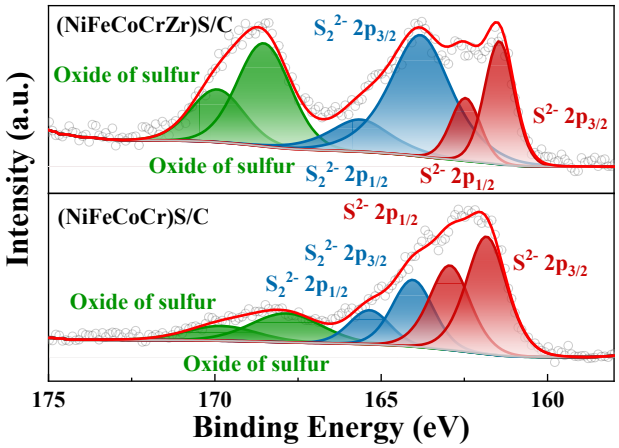

Figure S18 High-resolution S 2p core level XPS spectra of (NiFeCoCrZr)S/C and (NiFeCoCr)S/C.

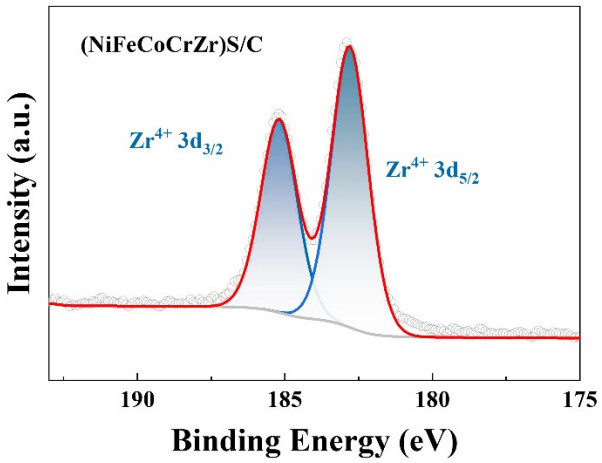

Figure S19 High resolution Zr 3d core level XPS spectrum of (NiFeCoCrZr)S/C.

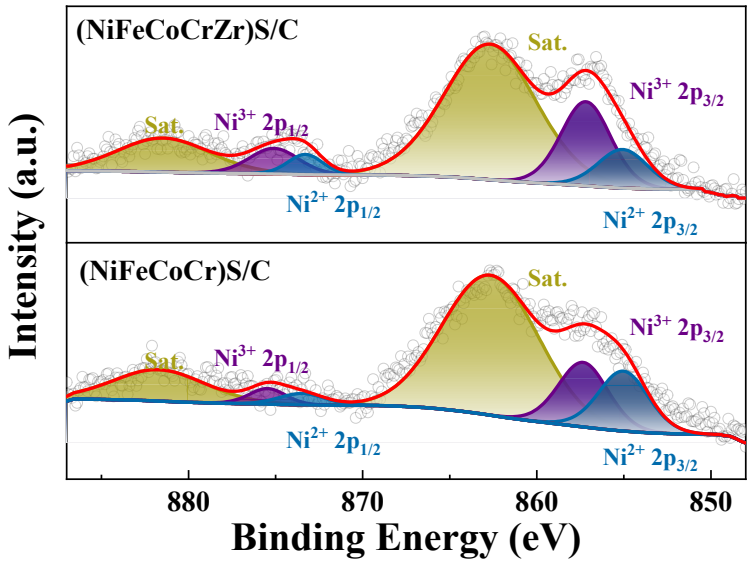

Figure S20 High resolution Ni 2p core level XPS spectra of (NiFeCoCrZr)S/C and (NiFeCoCr)S/C after OER test.

Table S1 The amount of the materials used in the synthesis.

Catalyst / Material	(Ni)S/C	(NiFe)S/C	(NiFeCo)S/C	(NiFeCoCr)S/C	(NiFeCoCrZr)S/C
Ketjen Black (EC-300) (mg)	73.4	96.6	121.2	142.8	180.8
L-Thioproline (mmol)	1.29	1.71	2.14	2.57	3.00
$Ni(NO_3)_2 \cdot 6H_2O$ (mmol)	0.75	0.75	0.75	0.75	0.75
$FeSO_4 \cdot 7H_2O$ (mmol)		0.25	0.25	0.25	0.25
$Co(NO_3)_2 \cdot 6H_2O$ (mmol)			0.25	0.25	0.25
$Cr(NO_3)_3 \cdot 9H_2O$ (mmol)				0.25	0.25
$Zr(NO_3)_4 \cdot 5H_2O$ (mmol)					0.25

Table S2 Mass content of the metals in (NiFeCoCrZr)S/C.

Element	Content (wt%)
Ni	11.0
Fe	3.7
Co	3.8
Cr	3.4
Zr	6.8

Table S3 OER performance of the reported high-entropy materials.

Catalyst	**η_{10} (mV)**	**Tafel slope ($mV \cdot dec^{-1}$)**	**Ref.**
(NiFeCoCrZr)S/C/NF	227	29.5	**This work**
$Al_{16.7}Fe_{16.7}Co_{16.7}Ni_{16.7}Cr_{16.7}Mn_{16.7}$	238	46.0	1
FeCoNiCrMo	282	55.8	2
GaFeCoNiCr HEO nanosheet	240	37.9	3
$(FeCoNiCrMn)_3O_4$ HEO	239	52.4	4
$FeCoNiMnCuBO_y$ HEO	259	74.8	5
FeCoNiCuMn	251	47.9	6
$NiCuCo^{II}$-$Fe^{III}Co^{III}$	288	97.0	7
NiFe-PBA@IF	253	47.9	8
ZnFeNiCoCr	315	86.7	9
FeCoNiMnW@CCC	253	41.0	10
$FeCoNiCrMo_{1.0}$	243	36.9	11
(FeCoNiCrCuAl)S@HCS	253	61.5	12
HES MoMn	288	43.6	13

Table S4 C_{dl}, ECSA, and J_{ECSA} at 1.5 V of the catalysts.

Catalyst	**C_{dl} ($mF \cdot cm^{-2}$)**	**ECSA (cm^2)**	**J_{ECSA} at 1.5 V ($\mu A \cdot cm^{-2}$)**
(Ni)S/C	16.4	411	3.26
(NiFe)S/C	16.9	422	9.47
(NiFeCo)S/C	22.1	552	12.9
(NiFeCoCr)S/C	22.0	550	18.2
(NiFeCoCrZr)S/C	25.8	644	30.0

Table S5 Metal dissolution in the electrolyte after 100 h of stability test for (NiFeCoCrZr)S/C and (NiFeCoCr)S/C measured by ICP-MS.

Elements	**C_x (μg·L^{-1})**	
	(NiFeCoCrZr)S/C	**(NiFeCoCr)S/C**
Ni	18.6	41.9
Fe	189.0	194.0
Co	1.4	2.6
Cr	116.7	164.4
Zr	66.8	

Reference

1. R. Y. Wu, R. Y. Gao, Z. B. Li, J. Wang, H. Wang, Y. Wu, S. H. Jiang, X. B. Zhang, X. Z. Wang, X. J. Liu and Z. P. Lu, *J. Mater. Sci. Technol*., 2025, **238**, 266–275.
2. F. H. Guo, X. Liu, S. Y. Chen, Y. T. Sun, X. Y. Chu, H. Xu, X. D. Meng, L. Yuan and Y. M. Zhang, *J. Alloys Compd.*, 2025, **1031**, 180844.
3. J. J. Liang, J. L. Liu, H. L. Wang, Z. Y. Li, G. H. Cao, Z. Y. Zeng, S. Liu, Y. Z. Guo, M. Q. Zeng and L. Fu, *J. Am. Chem. Soc.*, 2024, **146**, 7118–7123.
4. B. M. Feng, J. Chen, Y. F. Yang, C. Y. Zhong, X. C. Zhao and Y. X. Yao, *J. Materiomics*, 2024, **10**, 919–927.
5. S. D. Jiang, Y. H. Yu, H. He, Z. Y. Wang, R. G. Zheng, H. Y. Sun, Y. G. Liu and D. Wang, *Small*, 2024, **20**, 2310786.
6. J. Li, X. W. Wang, J. Q. Niu, S. Q. Li, C. W. Guo, Z. X. Qiu and S. Gao, *Int. J. Hydrogen Energy*, 2025, **113**, 385–394.
7. J. Li, M. Guo, X. Yang, J. L. Wang, K. X. Wang, A. R. Wang, F. C. Lei, P. Hao, J. F. Xie and B. Tang, *Prog. Nat. Sci.* 2022, **32**, 705–714.
8. L. H. Wei, D. X. Meng, J. H. Mao, Q. Q. Jiang, H. B. Huang and J. G. Tang, *Mol. C*atal., 2023, 544, 113126.
9. J. Li, B. Li, P. T. Li, N. Zhang and H. S. Shang, *Rare Met.*, 2025, **44**, 1789–1799.
10. C. M. Song, J. Wu, Y. Li, Z. T. Fang, F. Wang, F. B. Meng, J. Zhang and B. G. Shen, *Appl. Surf. Sci.*, 2024, **678**, 161088.
11. X. C. Zhou, H. Zhu, S. Fu, S. Lan, H. Hahn, J. R. Zeng and T. Feng, *Small*, 2024, **20**, 2405596.
12. Y. Wan, W. R. Wei, S. Q. Ding, L. Wu and X. X. Yuan, *Small*, 2024, **20**, 2404689.
13. L. Lin, Z. M. Ding, G. Karkera, T. Diemant, M. V. Kante, D. Agrawal, H. Hahn, J. Aghassi-Hagmann, M. Fichtner, B. Breitung and S. Schweidler, *Small Struct.*, 2023, **4**, 2300012.